Cell Trappable Quinoline-Derivatized Fluoresceins for Selective and Reversible Biological Zn(II) Detection

*Lindsey E. McQuade and Stephen J. Lippard**

Contribution from the Department of Chemistry, Massachusetts Institute of Technology, Cambridge, Massachusetts 02139

Email: lippard@mit.edu

RECEIVED DATE

TITLE RUNNING HEAD: Fluorescent Biological Zn(II) Dectection

ABSTRACT: The synthesis and spectroscopic characterization of two new, cell-trappable fluorescent probes for Zn(II) are presented. These probes, 2-(4,5-bis((6-(2-ethoxy-2-oxoethoxy)quinolin-8-yl)amino)methyl)-6-hydroxy-3-oxo-3*H*-xanthen-9-yl)benzoic acid (QZ2E) and 2,2′-((8,8′-(((9-(2-carboxyphenyl)-6-hydroxy-3-oxo-3*H*-xanthene-4,5-diyl)bis(methyl-ene))bis(azanediyl)bis(quinolin-8,6-diyl)}bis(oxy))diacetic acid (QZ2A), are poorly emissive in the off-state, but exhibit dramatic increases in fluorescence upon Zn(II) binding (120 ± 10-fold for QZ2E, 30 ± 7-fold for QZ2A). This binding is selective for Zn(II) over other biologically relevant metal cations, toxic heavy metals, and most first-row transition metals, and is of appropriate affinity (K_{d1} (QZ2E) = 150 ± 100 μM, K_{d2} (QZ2E) = 3.5 ± 0.1 mM, K_{d1} (QZ2A) = 220 ± 30 μM, K_{d2} (QZ2A) = 160 ± 80 μM, K_{d3} (QZ2A) = 9 ± 6 μM) to reversibly bind Zn(II) at physiological levels. In live cells, QZ2E localizes to the Gogli apparatus where it can detect Zn(II). It is cell membrane permeable until cleavage of its ester groups by intracellular esterases

produces QZ2A, a negatively charged acid form that cannot cross the cell membrane.

KEYWORDS: Zinc, cell-trappable sensor, fluorescence, binding constant

Introduction

Zinc is a ubiquitous and essential metal in biology. It is both tightly associated with proteins, where it plays structural and catalytic roles,[1] and loosely bound in pools of so-called "mobile zinc."[2] The latter occur in abundance in certain regions of the body, including the hippocampus[3] and olfactory bulb[4] in the brain, the mitochondria of the prostate,[5,6] and the pancreas,[7] where release of Zn(II) plays an important role in physiological signaling and other functions. As for any signaling molecule, maintaining homeostasis is critical to proper function, and zinc levels are highly regulated by transporters[2,8,9] and zinc-binding proteins, such as metallothionein.[10,11] Disruption of Zn(II) homeostasis has been associated with several pathologies, including ischemia,[12] Alzheimer's disease,[13,14] and prostate cancer.[15,16]

To understand the biological roles of mobile Zn(II) it is desirable to have tools for its detection in vivo.[17-21] Although many methods are available for sensing metal ions, fluorescence detection by microscopy has proved to be an invaluable technique for non-invasive imaging of mobile Zn(II). Fluorescent probes can be designed to be biologically compatible, that is, water-soluble, cell-membrane permeable, non-toxic, and excitable at low-energy wavelengths that do not induce interfering autofluorescence or harm the cell. Their photophysical properties can be tuned such that large differences occur in luminescence for the metal-free and metal-bound states, through changes in intensity and/or wavelength. Sensor characteristics such as binding affinity can be adjusted to match the physiological concentration of the analyte of interest and, in the case of metal ion sensing, the chelating group can be chosen to impart selectivity to the probe.

Many such Zn(II)-selective sensors have been designed and utilized for both ex vivo and in vivo imaging. Fig. 1 portrays a selection of symmetrical, fluorescein-based probes of this kind developed in our laboratory.[22-31] Fluorescein is an ideal reporter because it is biologically compatible, very bright in the

on-state (ϕ = 0.95 in 0.1 N NaOH),[32] and compatible with most fluorescent microscopes. The pH dependence of fluorescein can be modified such that proton-induced fluorescence enhancement of a probe is minimized at physiological pH.[23,27,33,34] Symmetrical sensors tend to have lower extinction coefficients than their asymmetrical counterparts, thereby lowering fluorescence emission in the metal-free state and increasing the effective dynamic range.[23,25]

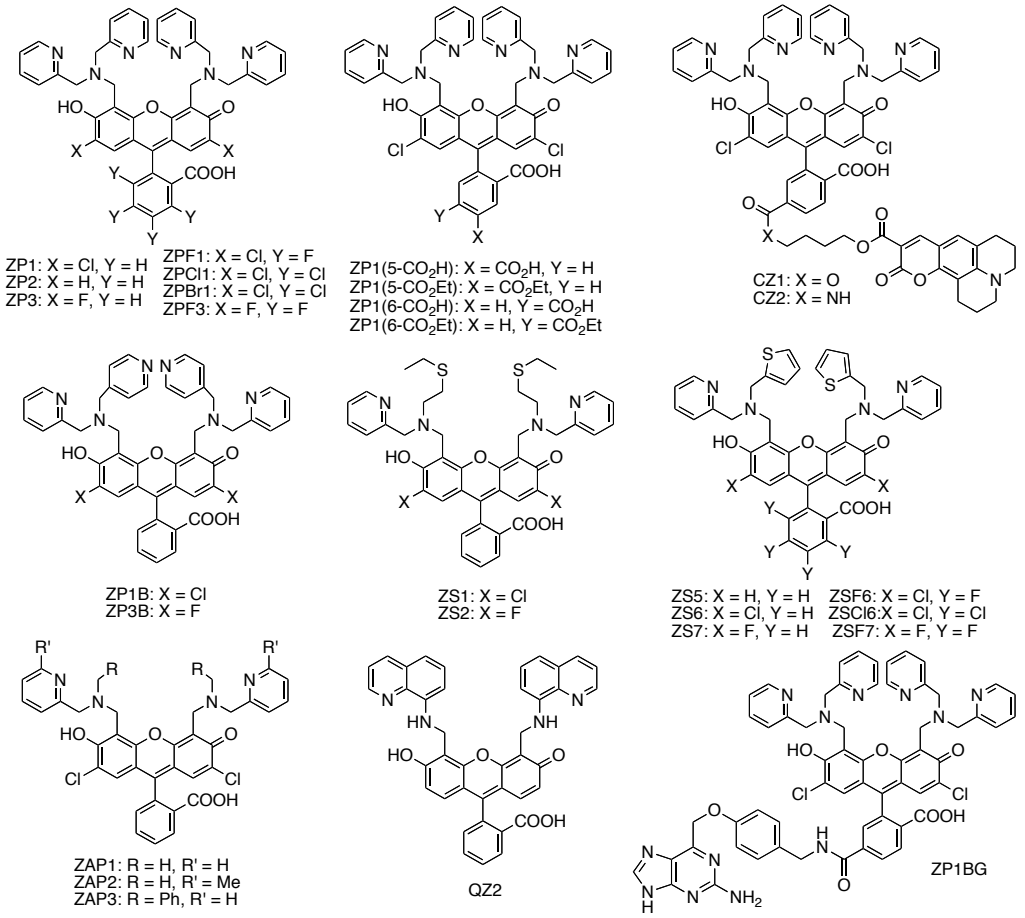

Figure 1. Select symmetrical, fluorescein-based Zn(II) probes.

One of the symmetrical probes illustrated in Fig. 1, QZ2,[25] displays particularly interesting sensing characteristics by comparison to the first generation Zinpyr (or ZP) family of probes.[22,23,28-31,35-39] For example, QZ2 has a much lower affinity for Zn(II) (K_{d1} ~ mid-micromolar) than ZP1 (K_{d1} ~ picomolar), and can therefore detect higher concentrations of mobile Zn(II) reversibly and without probe saturation. It also has a larger dynamic range (~ 150-fold turn on) than any of the ZP-type probes, which is beneficial for in vivo imaging, where poor signal-to-noise ratios can limit data interpretation. One limitation of

QZ2 is that it is not cell-trappable. Other similar quinoline-derivatized fluorescein probes, such as the NO sensor CuFL1,[40,41] readily diffuse out of cells after loading under continual perfusion of media. Because media flow is a requirement for many biological imaging experiments, a cell-trappable version of QZ2 would render it useful for more diverse sensing applications.

Herein we report the synthesis, photophysical characterization, and live-cell imaging of the desired new probe for Zn(II), QZ2E, which employs the ester/acid strategy for cell-trappability, as well as its cell-impermeable acid counterpart, QZ2A. QZ2E and QZ2A display dramatic fluorescence enhancements in the presence of excess Zn(II), which are selective for the metal over other biologically relevant alkali and alkaline earth metal ions, toxic heavy metal ions, and most first row transition metal ions. The binding of Zn(II) by QZ2E and QZ2A is weak with K_d values ranging from micromolar to millimolar, making the sensors suitable for detecting mobile Zn(II) at high physiological concentrations.

Experimental Section

Synthetic Materials and Methods. 4′,5′-Fluoresceindicarboxaldehyde[22] and ethylenediamine tetraacetate ethyl ester (EDTA-$(Et)_4$)[42] were prepared by previously reported procedures. All other chemicals were used as received. Silica gel (SiliaFlash F60, Silicycle, 230-400 mesh) was used for column chromatography. Thin-layer chromatography (TLC) was performed on EMD Chemicals F254 silica gel-60 plates (1 mm thickness), and viewed by either UV light or ninhydrin staining. ^{1}H and ^{13}C{^{1}H} NMR spectra were obtained on either a Varian 300 MHz or 500 MHz spectrometer. Chemical shifts are reported in parts per million (δ) and are referenced to residual protic solvent resonances. The following abbreviations are used in describing NMR couplings: (s) singlet, (d) doublet, (dd) doublet of doublets, (t) triplet, (q) quartet, (m) multiplet. High-resolution mass spectra were measured by staff at the MIT Department of Chemistry Instrumentation Facility (DCIF).

6-Hydroxy-8-nitroquinoline (1). 4-Amino-3-nitrophenol (5.00 g, 32.4 mmol) was suspended at 95 ^{O}C in 37% hydrochloric acid (35 mL) and 85% phosphoric acid (15 mL). Acrolein (2.4 mL, 36 mmol)

was added dropwise and the reaction mixture was stirred while heating for 4 h, during which time it changed color from yellow to orange to dark red. The reaction mixture was cooled, filtered, and washed with water. Ammonium hydroxide (28%, 50 mL) was added to the filtrate and the resulting red precipitate was filtered and washed with water to yield pure product (1.11 g, 18%). TLC R_f = 0.68 (silica, 9:1 CH_2Cl_2:CH_3OH); mp: 162 – 163 ºC (dec); ^{1}H NMR (DMSO-d_6, 300 MHz) δ: 7.45 (1H, d, J = 2.7 Hz), 7.58 (1H, dd, J = 8.4 Hz, 4.2 Hz), 7.80 (1H, d, 2.7 Hz), 8.35 (1H, dd, J = 8.4 Hz, 1.2 Hz), 8.78 (1H, dd, J = 4.2 Hz, 1.8 Hz); ^{13}C{^{1}H} NMR (DMSO-d_6, 125 MHz) δ: 112.34, 115.45, 123.19, 129.82, 133.50, 134.76, 148.63, 149.34, 154.42; HRMS (m/z): $[M + H]^+$ calcd 191.0451, found 191.0450.

Ethyl[(8-aminoquinolin-6-yloxy)acetate] (2). To a solution of 6-hydroxy-8-nitroquinoline (**1**, 234 mg, 1.23 mmol) in ethanol (10 mL) was added ethylbromoacetate (400 μL, 3.6 mmol) and *N,N*-diisopropylethylamine (650 μL, 3.7 mmol) and the reaction was heated to reflux for 24 h. The reaction was then cooled and the solvent removed. The resultant crude product was taken up in fresh ethanol (25 mL) containing 10% palladium on carbon (203 mg) and purged with N_2 for 15 min, after which an atmosphere of H_2 was applied and the reaction was stirred at room temperature for 16 h. The resulting solution was then purged with N_2, filtered, and the solvent was removed. The dark brown solid was purified by column chromatography on silica using 3:1 hexanes:ethyl acetate as the eluant to afford a pure, light brown solid (227 mg, 75%). TLC R_f = 0.20 (silica, 1:1 Hex:EtOAc); mp: 92 – 94 ºC; ^{1}H NMR (CD_2Cl_2, 300 MHz) δ: 1.29 (3H, t, J = 7.2 Hz), 4.26 (2H, q, J = 7.2 Hz), 4.69 (2H, s), 5.08 (2H, broad s), 6.39 (1H, d, J = 2.7 Hz), 6.61 (1H, d, J = 2.4 Hz), 7.33 (1H, dd, J = 8.4, 4.2 Hz), 7.95 (1H, dd, J = 8.4 Hz, 1.5 Hz), 8.59 (1H, dd, J = 4.2 Hz, 1.5 Hz; ^{13}C{^{1}H} NMR (CD_2Cl_2, 125 MHz) δ: 14.51, 61.84, 65.78, 95.62, 101.40, 122.51, 130.12, 135.34, 135.97, 145.97, 146.16, 157.58, 169.22; HRMS (m/z): $[M + H]^+$ calcd 247.1077, found 247.1079.

2-(4,5-Bis(((6-(2-ethoxy-2-oxoethoxy)quinolin-8-yl)amino)methyl)-6-hydroxy-3-oxo-3*H*-xanthen-9-yl)benzoic acid (QZ2E, 3). 4′,5′-Fluoresceindicarboxaldehyde (43.9 mg, 113 μmol) and ethyl[(8-aminoquinolin-6-yloxy)acetate] (**2**, 54.8 mg, 223 μmol) were suspended in methanol (5 mL) and stirred

at room temperature for 1 h. The dark red suspension was cooled to 0 ºC and sodium borohydride (21.5 mg, 568 μmol) was added. The reaction clarified to a dark red solution, which was stirred for 1 h as it warmed to room temperature. The reaction solution was quenched with water (5 mL) and the methanol was removed under reduced pressure. The aqueous phase was extracted with 5 x 10 mL of dichloromethane and the combined extracts were dried over $MgSO_4$, filtered, and the solvent was removed. The resulting residue was purified by column chromatography on silica (gradient from 99:1 CH_2Cl_2:CH_3OH to 19:1 CH_2Cl_2:CH_3OH) to afford a dark red solid (25.6 mg, 27%). TLC R_f = 0.67 (silica,); mp: 148 – 149 ºC; ^{1}H NMR (DMSO-d_6, 500 MHz) δ: 1.19 (6H, t, *J* = 4.2 Hz), 4.16 (4H, q, *J* = 8.4 Hz, 4.2 Hz), 4.75 (4H, s), 4.79 (4H, d, *J* = 3.6 Hz), 6.40 (2H, d, *J* = 1.5 Hz), 6.53 (2H, d, *J* = 5.4 Hz), 6.66 (2H, d, *J* = 1.5 Hz), 6.71 (2H, d, *J* = 5.4 Hz), 6.77 (2H, t, *J* = 3.3 Hz), 7.34 (1H, d, *J* = 4.5 Hz), 7.37 (2H, dd, *J* = 4.8 Hz, 2.4 Hz), 7.74 (2H, dt, *J* = 12 Hz, 4.2 Hz), 7.98 (1H, d, *J* = 4.5 Hz), 8.02 (2H, d, *J* = 4.8 Hz), 8.48 (2H, d, *J* = 2.4 Hz); ^{13}C{^{1}H} NMR (DMSO-d_6, 125 MHz) δ: 13.98, 14.13, 60.62, 64.61, 77.13, 83.42, 93.18, 93.38, 96.26, 96.43, 109.90, 111.96, 122.14, 124.66, 126.31, 127.05, 127.73, 129.13, 130.14, 134.65, 134.87, 145.28, 150.49, 152.08, 157.19, 157.56, 168.55, 168.61; HRMS (m/z): $[M + Na]^+$ calcd, 871.2586, found 871.2570.

Synthesis of 2,2′-((8,8′-(((9-(2-carboxyphenyl)-6-hydroxy-3-oxo-3*H*-xanthene-4,5-diyl)bis(methylene))bis(azanediyl))bis(quinolin-8,6-diyl))bis(oxy))diacetic acid (QZ2A, 4). QZ2E (121.9 mg, 144 μmol) was dissolved in aqueous sodium hydroxide (0.5 N, 15 mL) and methanol (5 mL) and heated to 90 ºC for 12 h. The solution was cooled to room temperature and the pH was adjusted with concentrated hydrochloric acid until an orange precipitate formed. The solid was filtered, washed with water, and dried to yield the product (77.6 mg, 68%). TLC R_f = 0.63 (silica, 100% CH_3OH); mp: 139 – 141 ºC (dec); ^{1}H NMR (DMSO-d_6, 300 MHz) δ: 4.62 (4H, s), 4.71 (4H, s), 6.46 (2H, s), 6.50 (2H, s), 6.59 (2H, d, *J* = 8.7 Hz), 6.75 (2H, d, *J* = 8.4 Hz), 7.39 – 7.42 (3H, m), 7.70 – 7.82 (2H, m), 8.00 (2H, d, *J* = 7.2 Hz), 8.17 (2H, d, *J* = 7.8 Hz), 8.44 (2H, d, *J* = 3.9 Hz), 10.55 (2H, broad s); ^{13}C{^{1}H} NMR (DMSO-d_6, 125 MHz) δ: 36.40, 64.51, 93.39, 93.76, 98.31, 109.80, 111.22, 112.27, 121.85, 122.20, 124.33, 124.70,

126.10, 127.59, 127.91, 129.70, 130.16, 130.37, 135.62, 142.83, 143.67, 150.61, 152.52, 157.75, 168.78, 169.96; HRMS (m/z): $[M - H]^-$ calcd 791.1995, found 791.1994.

Spectroscopic Materials and Methods. Piperazine-*N*,*N*′-bis(2-ethanesulfonic acid) (PIPES) was purchased from Calbiochem. Potassium chloride (99.999%) was obtained from Aldrich. Buffer solutions (50 mM PIPES, 100 mM KCl, pH 7) were prepared in Millipore water, chelexed, filtered, and used for all spectroscopic studies. Zinc chloride (Aldrich, 99.999%) stock solutions of 1 M, 100 mM, 10 mM, and 1 mM were prepared in Millipore water. Stock solutions of 1 mM ligands were prepared in DMSO and stored in aliquots at -80 ºC. Stock solutions of 40 mM ethylenediamine tetraacetate (EDTA) and 40 mM *N*,*N*,*N*′,*N*′-tetrakis(2-pyridylmethyl)-ethylenediamine (TPEN) were prepared in DMSO, aliquotted, and stored at -20 ºC. UV-visible spectra were acquired on a Cary 50-Bio spectrometer using spectrosil quartz cuvettes from Starna cells Inc. (3.5 mL volume, 1 cm path length). Acquisitions were made at 25.00 ± 0.05 ºC. Fluorescence spectra were obtained on a Quanta Master 4L-format scanning spectrofluorimeter (Photon Technology International) at 25.0 ± 0.1 ºC using 1 μM QZ2E or QZ2A unless otherwise noted. All fluorescence experiments were repeated in triplicate.

Cell Culture and Imaging Materials and Methods. HeLa cells were obtained from American Type Cell Collection (ATCC) and cultured in Dulbecco's Modified Eagle Medium (DMEM, Cellgro, MediaTek, Inc.) supplemented with 10% fetal bovine serum (FBS, PAA Laboratories), 2 mM glutamine (GIBCO, Invitrogen), 100 U/mL penicillin (Cellgro, MediaTek, Inc.), and 100 μg/mL streptomycin (Cellgro, MediaTek, Inc.). For imaging studies, cells were plated in poly-D-lysine coated plates (MatTek) containing 2 mL of complete DMEM and incubated overnight at 37 ºC under 5% CO_2.

For Zn(II) detection studies, the HeLa cells were incubated with 5 μM QZ2E or QZ2A for ~ 18 h. Thirty minutes prior to imaging, the cells were co-incubated with 4.5 μM Hoechst 33258 (Sigma), and either 200 nM Mitotracker Red (Invitrogen) or 100 nM BOPIDY TR Ceramide (Invitrogen) for 30 min. Cells were washed twice with 1 mL of phosphate buffered saline (PBS, Cellgro, MediaTek, Inc.) before

imaging and then bathed in 2 mL of serum-free DMEM during imaging. Stock solutions of 10 mM $ZnCl_2$, prepared in Millipore water, and 20 mM sodium pyrithione (2-pyridinethiol-1-oxide), prepared in DMSO, were combined in a 1:1 ratio and diluted in serum-free DMEM to a 5 mM stock concentration. Zn(II) was added to cells directly on the microscope stage at a final concentration of 100 μM and allowed to incubate with cells for 5 min prior to imaging. Stock solutions of 40 mM ethylenediamine tetraacetate ethyl ester (EDTA-$(Et)_4$)[42] and 40 mM *N*,*N*,*N*′,*N*′-tetrakis(-)[(2-pyridylmethyl)]-ethylenediamine (TPEN) were prepared in DMSO, aliquotted, and stored at -20 ºC. Aliquots were thawed immediately prior to use and diluted in serum-free DMEM to a 4 mM stock concentration. The chelators were added to the cells on the microscope stage at a final concentration of 150 μM for 5 min prior to imaging.

For diffusion studies, HeLa cells were incubated with 5 μM QZ2E for 18 h, with 4.5 μM Hoechst 33258 added 30 min prior to imaging for nuclear staining. Cells were washed twice with 1 mL of PBS prior to imaging and then bathed in 2 mL of serum-free DMEM during imaging. To mimic media flow, the serum-free DMEM was removed, and the cells were washed three times with 1 mL of fresh serum-free DMEM and then bathed in 2 mL of fresh serum-free DMEM. This process was repeated every 10 min during imaging.

Images were acquired on a Zeiss Axiovert 200M inverted epifluorescence microscope equipped with an EM-CCD digital camera (Hamamatsu) and a MS200 XY Piezo Z stage (Applied Scientific Instruments), illuminated by an X-Cite 120 metal-halide lamp (EXFO). Plates were maintained on the microscope stage in an INC-2000 incubator kept at 37 ºC under 5% CO_2. Differential interference contrast (DIC) and red, blue, and green fluorescent images were obtained using an oil immersion 63x objective lens, with 2.00 s exposure times for green fluorescent images. The microscope was operated with Volocity software (Improvision). All fluorescent images were corrected for background.

Cytotoxicity Assays. HeLa cells were seeded into 96-well plates (100 μL total volume/well, 2500 cells/well) in complete DMEM and incubated at 37 ºC under 5% CO_2 for 24 h. The medium was re-

placed and the cells incubated with QZ2E (1 μM – 50 μM, with an untreated control lane and a 5% DMSO in complete DMEM lane) for another 24 h. The medium was removed and replaced with 200 μL of a 20:1 mixture of FBS-free DMEM and (3-(4,5-dimethylthiazol-2-yl)-2,5-diphenyltetrazolium bromide (MTT, 5 mg/mL stock in PBS). The cells were incubated for 4 h and then the medium was removed and replaced with DMSO (100 μL/well). The absorbance of each well was recorded at 555 nm on a microplate reader (BioTek, Synergy HT) and the percent cell survival values are reported relative to those of untreated control cells.

Results and Discussion

Design Considerations. The new trappable Zn(II) probes were based on the QZ2 scaffold, because this ligand offers many advantages as a Zn(II) detector.[25] Firstly, it employs fluorescein as the reporter, which imparts good sensing characteristics (vide supra). Secondly, QZ2 detects Zn(II) with av ~ 150-fold dynamic range, and is selective for Zn(II) over most biologically relevant cations, toxic heavy metals, and first-row transition metal ions, with the exception of Cu(II) and Ni(II), neither of which is available as a mobile M(II) species at high concentrations in vivo. Lastly, QZ2 is capable of detecting Zn(II) using one- and two-photon fluorescence microscopy in live cells, where it reports variable fluorescence over a wide range of Zn(II) concentrations. Importantly, the low binding affinity of QZ2 (dissociation constant K_{d1} = 41 ± 3 μM)[25] relative to other Zn(II)-specific probes such as ZP1 (K_{d1} = 0.04 pM, K_{d2} = 1.2 nM)[39] make QZ-type probes suitable for in vivo imaging under conditions of high zinc levels, such as in synaptic clefts during neurotransmission in the hippocampus[43,44] or from the pancreatic beta cells during insulin secretion,[45] where it is estimated that labile Zn(II) concentrations may approach millimolar concentrations. Because QZ2 binds Zn(II) with a micromolar dissociation constant and its fluorescence does not saturate until millimolar concentrations of Zn(II) are present, QZ2 Zn(II) binding and subsequent fluorescence enhancement should be reversible under these physiological conditions, mak-

ing the probe particularly suitable for in vivo imaging.

To impart cell-trappability to QZ2, esters were incorporated onto the quinoline rings. Esters maintain cell permeability until the probe is internalized by cells, where intracellular esterases hydrolyze the substituents to negatively charged carboxylates. The two negative charges on the probe scaffold make QZ2E incapable of re-crossing the cell membrane, rendering it cell-trappable.

Synthesis. The synthetic routes to QZ2E and QZ2A are presented in Scheme 1. 6-Hydroxy-8-nitroquinoline, **1**, was prepared in low yield by the Skraup-Doebner-von Miller reaction between acrolein and 4-amino-3-nitrophenol. Esterification of the quinoline using ethyl bromoacetate and Hünig's base, followed by reduction of the nitro group by hydrogenation with palladium on carbon afforded ethyl[(8-aminoquinolin-6-yloxy)acetate], **2**, in moderate yield. Condensation of the aminoquinoline with 4′,5′-fluoresceindicarboxaldehyde[22] in methanol followed by reduction of the imine using sodium borohydride resulted in product formation. Purification by column chromatography on silica afforded the trappable ligand, QZ2E, **3**, in fair yield. Subsequent hydrolysis of QZ2E using aqueous sodium hydroxide in methanol and precipitation with acid afforded the cell-impermeable ligand, QZ2A, **4**, in moderate yield without the need for further purification.

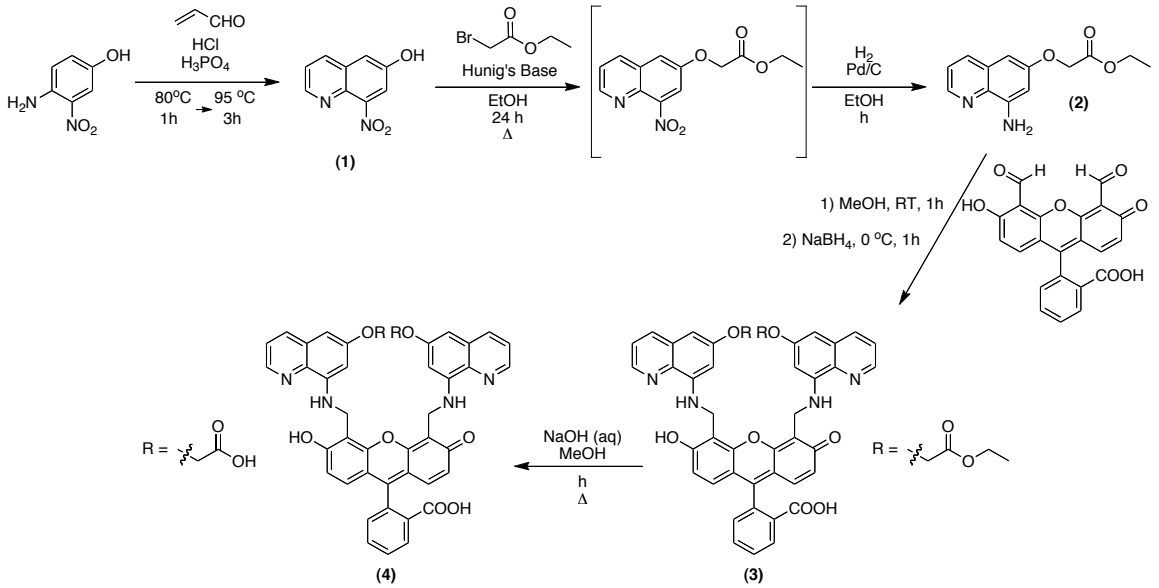

Scheme 1. Syntheses of QZ2E and QZ2A.

Spectroscopic Properties of QZ2E and QZ2A. QZ2E and QZ2A exhibit spectroscopic features similar to those of QZ2 (Table 1).[25] The absorbance spectral maxima occur at 499 nm for QZ2E (ε = 2.72 ± 0.09 x 10^4 $M^{-1}cm^{-1}$) with a shoulder at 467 nm (ε = 1.2 ± 0.2 x 10^4 $M^{-1}cm^{-1}$), and at 498 nm for QZ2A (ε = 6.41 ± 0.03 x 10^4 $M^{-1}cm^{-1}$) with a shoulder at 464 nm (ε = 2.49 ± 0.2 x 10^4 $M^{-1}cm^{-1}$). Upon addition of excess $ZnCl_2$, the maximum absorbance shifts hypsochromically to 489 nm, 496 nm, and 492 nm (ε = 3.36 x 10^4 $M^{-1}cm^{-1}$, ε = 1.6 ± 0.3 x 10^4 $M^{-1}cm^{-1}$, and ε = 4.0 ± 0.2 x 10^4 $M^{-1}cm^{-1}$ for QZ2, QZ2E, and QZ2A, respectively) (Fig. S1). This blue-shift is typical for metal coordination by fluorescein-based sensors and is presumably caused by perturbation of the fluorescein π-system upon cation binding to the phenolic oxygen atoms of the xanthenone ring.

Table 1. Photophysical properties QZ2, QZ2E, and QZ2A.

	Absorbance λ (nm), ε x 10^4 ($M^{-1}cm^{-1}$)		Emission λ (nm), ϕ (%)[b]			
	unbound	Zn(II)	unbound	Zn(II)[c]	DR[d]	ref
QZ2[a]	499, 3.72	489, 3.36	~ 520, 0.5	518, 70	~ 150	23
QZ2E	499, 2.72(9)	496, 1.6(3)	519, 0.4(1)	514, 73(3)	120(10)	this work
QZ2A	498, 6.41(3)	492, 4.0(2)	515, 1.2(1)	515, 51(1)	30(7)	this work

[a] Measurements were performed in 50 mM PIPES, 100 mM KCl at pH 7.0. [b] Referenced to fluorescein (ϕ = 0.95 in 0.1 N NaOH). [c] 20 mM $ZnCl_2$ was added. [d] DR is the dynamic range, I_{NO}/I_o.

Esterified ligands get hydrolyzed during studies of their pH-dependent properties. We therefore did not attempt to measure the pK_a values of QZ2E. The pK_a of the secondary amine nitrogen atom of QZ2 is 7.0,[25] and an NO probe with a similar structure, FL2,[46] has the same pK_a value. Because of this similarity, it is likely that QZ2A and FL2A have comparable pK_a values (pK_a FL2A = 5.9). For QZ2, FL2, and FL2A, protonation causes only an ~ 2-fold increase in fluorescence, indicating that the ligands are fairly insensitive to pH in the biologically relevant range, especially by comparison to Zn(II)- or NO-promoted turn-on.

Metal binding of QZ2E and QZ2A. The emission profiles of QZ2E and QZ2A are almost identical to that of QZ2. The emission maxima and quantum yields of the free ligands are given in Table 1. Buff-

ered solutions of QZ2E exhibit significant fluorescence enhancements when treated with excess $ZnCl_2$, leading to a 120 ± 10-fold increase in integrated emission upon saturation and a quantum yield increase to 73% (Fig. 2a, Table 1). By comparison, addition of excess Zn(II) to QZ2 causes an ~ 150-fold increase in integrated emission and a quantum yield increase to 70%. The differences in fluorescent dynamic range can be accounted for by the difference in molar absorptivities of the two ligands. Comparing the product of the molar absoprtivity and quantum yield (ε x ϕ) of QZ2E (~ 114 $M^{-1}cm^{-1}$ in the off-state, ~ 11680 $M^{-1}cm^{-1}$ in the on-state) with that of QZ2 (~ 186 $M^{-1}cm^{-1}$ in the off-state, ~ 23520 $M^{-1}cm^{-1}$ in the on-state) yields dynamic ranges ((ε x ϕ) on/(ε x ϕ) off) of ~ 102 and ~ 126, respectively. The dynamic ranges observed by fluorescence (~ 120 and ~ 150, respectively) are larger, but the ratio of the dynamic range of QZ2E to that of QZ2 is ~ 0.8 using either (ε x ϕ) or fluorescence emission. Therefore, the difference observed is accounted for by the differences in molar absorptivities. Despite the slight lowering of dynamic range upon esterification of the quinoline, an ~ 120-fold change in fluorescence intensity is still much greater than that exhibited by Zn(II) sensors of the ZP family[19] and more than adequate for cellular imaging. Hydrolysis of QZ2E to QZ2A causes a significant reduction in dynamic range upon exposure to excess Zn(II) (30 ± 7-fold increase in integrated emission, Fig. 2b) because both

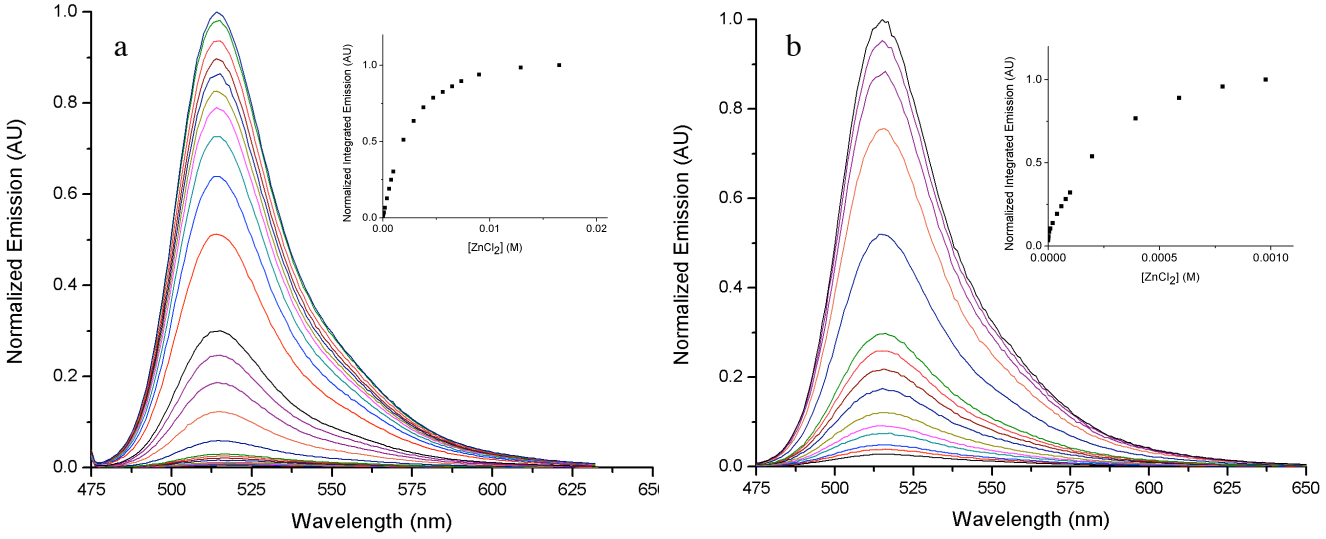

Figure 2. Normalized fluorescence response in the presence of excess $ZnCl_2$ of a) 1 μM QZ2E, 0 – 20 mM $ZnCl_2$ and b) 1 μM QZ2A, 0 – 1 mM $ZnCl_2$ in 50 mM PIPES, 100 mM KCl, pH 7.0, T = 25 ºC. Insets: Integrated fluorescence vs. $ZnCl_2$ concentration, normalized and adjusted for the basal fluorescence of the sensor in the absence of Zn(II).

the molar absorptivity and quantum yield of apo-QZ2A are significantly higher that those of either QZ2 or QZ2E. The quantum yield of the Zn(II)-saturated QZ2A is also lowered to 51% versus ~ 70% for QZ2 and QZ2E; however, a 30-fold turn-on is significantly greater than that of many useful Zn(II)-specific probes such as ZP1,[22] and is more than sufficient for live-cell imaging.

The strength of Zn(II) binding by a probe is an important feature that determines its use under specific biological conditions. Because biological mobile Zn(II) concentrations vary widely depending on location and physiological events, it is essential to have fluorescent sensors with a wide array of dissociation constants for Zn(II) in order to ensure reversible detection without probe saturation. As discussed in the design considerations, the QZ-type probes are weak Zn(II) binders, with K_d values in the micromolar range.[25] This affinity holds true for QZ2E, which requires millimolar Zn(II) for saturation of the fluorescence emission. The strength of QZ2E Zn(II) binding was determined by fitting the fluorescence data to a two-site model according to eq 1, where [Zn(II)] is the concentration of free Zn(II) corrected for dilu-

$$F = \frac{[QZ2E]_t(I_1+I_2K_{a1}[Zn(II)]+I_3K_{a1}K_{a2}[Zn(II)]^2)}{(1+K_{a1}[Zn(II)]+K_{a1}K_{a2}[Zn(II)]^2)} \quad (1)$$

tion, $[QZ2E]_t$ is the total concentration of the probe corrected for dilution, K_{a1} and K_{a2} are the association constants for the reactions in eqs 2 and 3, respectively, and I_1, I_2, and I_3 are the proportionality constants

$$QZ2E + Zn(II) \underset{}{\overset{K_{a1}}{\rightleftharpoons}} QZ2E(Zn(II)) \ , \ K_{a1} = \frac{[QZ2E(Zn(II))]}{[QZ2E][Zn(II)]} = 1/K_{d2} \quad (2)$$

$$QZ2E(Zn(II)) + Zn(II) \overset{K_{a2}}{\rightleftharpoons} QZ2E(Zn(II))_2 \ , K_{a2} = \frac{[QZ2E(Zn(II))_2]}{[QZ2E(Zn(II))][Zn(II)]} = 1/K_{d1} \quad (3)$$

$$F = I_1[QZ2E] + I_2[QZ2E(Zn(II))] + I_3[QZ2E(Zn(II)_2] \quad (4)$$

$$[QZ2E]_t = [QZ2E] + [QZ2E(Zn(II))] + [QZ2E(Zn(II)_2] \quad (5)$$

that account for the relative contributions of each QZ2E species to the overall fluorescence emission, according to eq 4 (Fig. 2, inset). Eq 1 was determined by substituting into eq 4, using eqs 2, 3, and 5. Because the binding of Zn(II) by QZ2E is weak, [Zn(II)] can be approximated by $[Zn(II)]_t$, the total concentration of Zn(II) corrected for dilution. Applying the fit to the normalized fluorescence data yields values of K_{a1} = 7000 ± 5000 M and K_{a2} = 287 ± 8 M. Substituting into eqs 2 and 3 yields dissociations constants of K_{d1} = 3.5 ± 0.1 mM (from K_{a2}) and K_{d2} = 150 ± 100 μM (from K_{a1}). The large error associated with the K_{a1} determination is probably due to the small changes in fluorescence intensity observed upon coordination of the first Zn(II) equivalent (Fig. S2a, micromolar region), a postulate substantiated by the fact that the second proportionality constant, I_2, is similar to the first (I_1 = 1.1 ± 0.3 x 10^4, I_2 = 3 ± 4 x 10^4) and that this value is subject to a large error. On the other hand, the large fluorescence changes associated with the second binding event (I_3 = 1.44 ± 0.01 x 10^6, Fig. S2a, millimolar region) allow for a more precise estimation of K_{a2}. It is useful to note that the order of magnitude of binding, ~ 100 μM, is of the same order as that estimated for QZ2. The K_{d1} value for QZ2 was determined by taking kinetic data measured by stopped-flow spectroscopy and fitting it to a one-site binding model, assuming that the second Zn(II) binding event is of significantly lower affinity. When the fluorescence data obtained for QZ2E were fit to a one-site model (eq 6), the K_d value was 2.9 mM, suggesting that the

$$F - F_0 = \frac{[QZ2E]_t(I_2-I_1)[Zn(II)]}{K_d + [Zn(II)]} \qquad (6)$$

second binding event is responsible for most of the fluorescence enhancement. The poor data fit, however, indicates that a one-site model is inadequate to describe the system (Fig. S2b).

When the same analysis was repeated for QZ2A using the two-site model, the data could not be fit within a reasonable degree of error (K_{d1} = 2 mM ± 9 mM, K_{d2} = 400 μM ± 300 μM, Fig. S3a). A three-site model was therefore employed, as described by eq 7, because a similar ligand diacid such as one in

$$F = \frac{[QZ2E]_t(I_1+I_2K_{a1}[Zn(II)]+I_3K_{a1}K_{a2}[Zn(II)]^2+I_4K_{a1}K_{a2}K_{a3}[Zn(II)]^3)}{(1+K_{a1}[Zn(II)]+K_{a1}K_{a2}[Zn(II)]^2+K_{a1}K_{a2}K_{a3}[Zn(II)]^3)} \qquad (7)$$

the Cu(II)-binding NO probe FL2A binds a third metal cation.[47] Fitting the fluorescence data for QZ2A to eq 7 gave three values of K_{d1} = 220 ± 30 μM, K_{d2} = 160 ± 80 μM, and K_{d3} = 9 ± 6 μM, all of which have a significant error, but the result was much better than that afforded by a two-site model (Fig. S3b). Most importantly, although Zn(II) binding strength to the quinoline pockets cannot be distinguished from Zn(II) affinity for the diacids, all K_d values are around the same order of magnitude as that of QZ2E (~ 100 μM) and appropriate for reversible Zn(II) sensing at physiological concentrations.

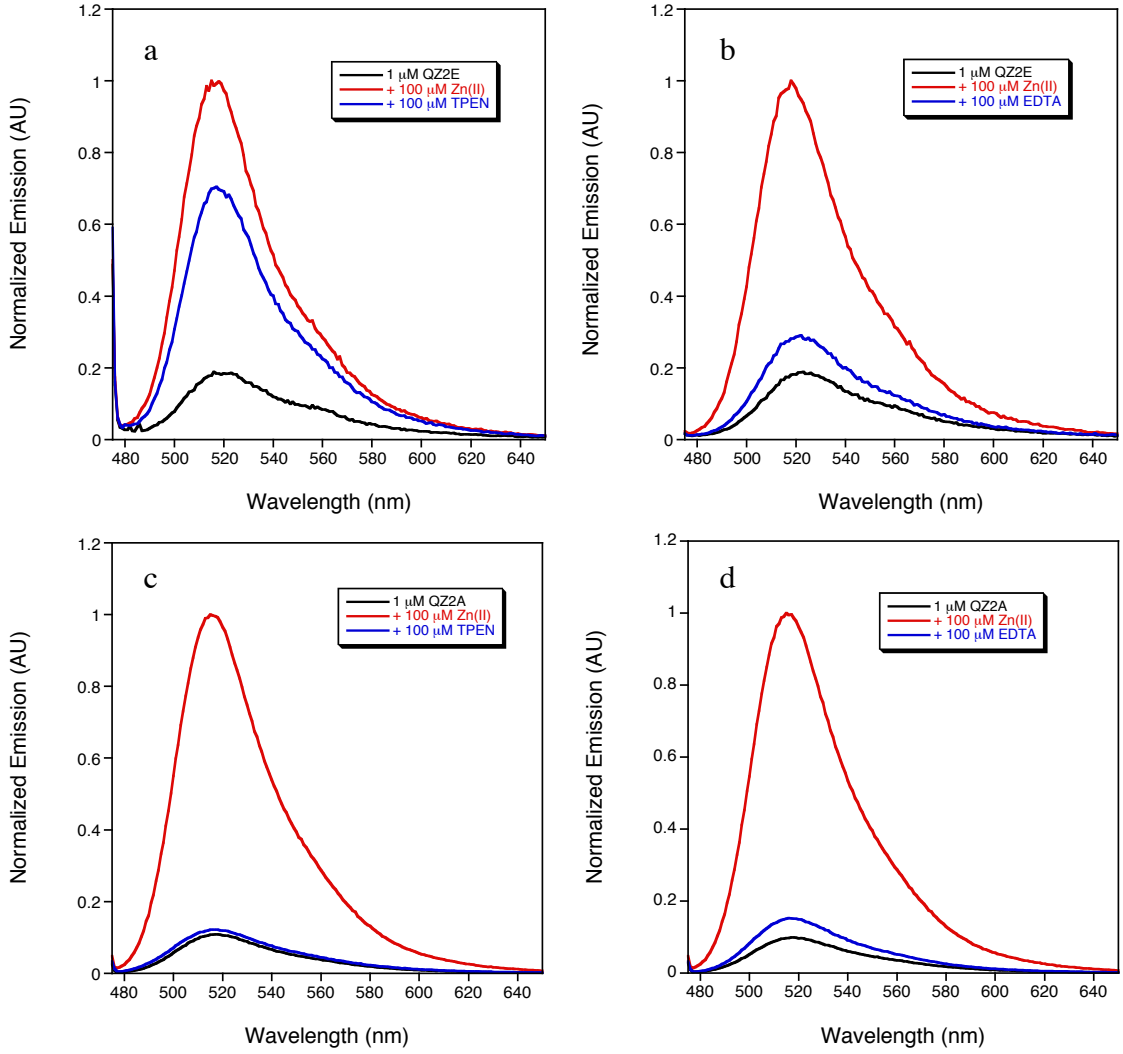

Figure 3. a) Normalized fluorescence response of 1 μM QZ2E to 100 μM TPEN after fluorescence is elicited by addition of 100 μM $ZnCl_2$, b) 1 μM QZ2E to 100 μM EDTA after fluorescence is elicited by addition of 100 μM $ZnCl_2$, c) 1 μM QZ2A to 100 μM TPEN after fluorescence is elicited by addition of 100 μM $ZnCl_2$, and d) 1 μM QZ2A to 100 μM EDTA after fluorescence is elicited by addition of 100 μM $ZnCl_2$.

Finally, because of the micromolar to millimolar affinity of QZ2E and QZ2A for Zn(II), it was ex-

pected that, like QZ2, their Zn(II)-induced fluorescence would be readily reversed by the Zn(II) chelator TPEN ($K_d = 10^{-15.6}$ M).[48] When 100 μM $ZnCl_2$ was added to a 1 μM solution of QZ2E, however, the resulting fluorescence was bearly affected by the addition of 100 μM TPEN (Fig. 3a). When the same experiment was repeated using EDTA ($K_d = 10^{-16.4}$ M)[48] as the Zn(II) chelator, the fluorescence was diminished to near baseline levels (Fig. 3b). Repeating the experiment with tripicolylamine (TPA) vs diethylenetriaminepentaacetic acid (DTPA, $K_d = 10^{-18.7}$ M)[48] gave similar results (data not shown). It is unlikely that TPEN and TPA are incapable of chelating Zn(II), given their superior affinity for the metal ion over QZ2E. The basic, pyridyl-based chelators seemingly interact with QZ2E to elicit a fluorescence response by a different, unknown mechanism. Because esterification of the quinoline rings of QZ2E presumably bends the quinolines out of plane with respect to the fluorescein to avoid a steric clash, it is possible that the Zn(II)-binding pocket of QZ2E is different from that of QZ2. We hypothesize that instead of chelating Zn(II), the pyridine rings of TPEN form a complex with Zn(II)-bound QZ2E, thereby stabilizing a fluorescent species. By comparison, the Zn(II)-induced fluorescence of QZ2A is fully reversed by both TPEN and EDTA (Fig. 3c, d), suggesting that removal of the ethyl groups is sufficient to relieve the purported steric clash. Because an effective chelator (EDTA) was found for QZ2E, TPEN binding was not further pursued.

Selectivity of QZ2E and QZ2A for Zn(II). In order for a probe to be useful for cellular detection of an analyte, it must be specific for that analyte over other competing biologically relevant species. One advantage of the QZ scaffold over the ZP scaffold is that, although the dipicolylamine chelating unit of the ZP family binds Zn(II) very tightly, it is not as specific for Zn(II) compared to the aminoquinoline Zn(II)-binding unit of QZ2.[19,25] Both families of sensors are specific for Zn(II) over the biologically relevant Na(I), Ca(II), and Mg(II), the first row transition element Mn(II), and the toxic heavy metals Hg(II) and Cd(II). The QZ family, however, is also selective for Zn(II) over Fe(II) and Co(II).[25] We therefore performed a fluorescence selectivity study to ensure that modification of the quinoline ring did not alter the metal binding properties of QZ2E or QZ2A significantly enough to affect its selectivity

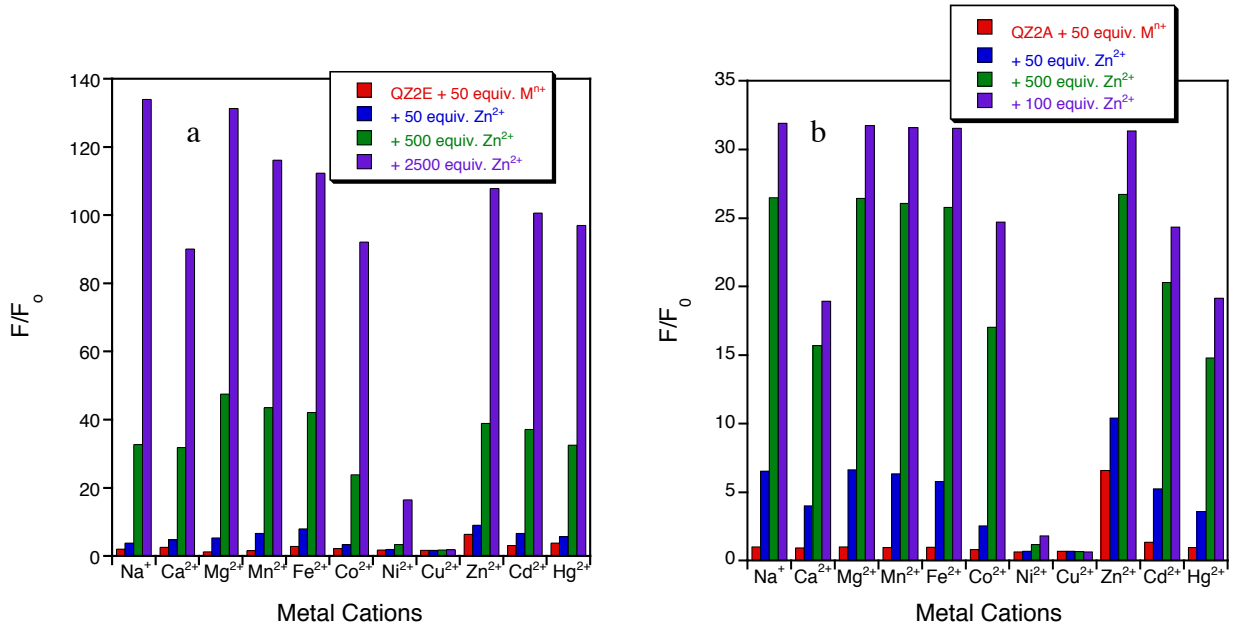

Figure 4. Selectivity of a) QZ2E and b) QZ2A for Zn(II) compared to Na(I), Ca(II), Mg(II), Mn(II), Fe(II), Co(II), Ni(II), Cu(II), Cd(II), and Hg(II). Normalized fluorescence response relative to the emission of QZ2E in 50 mM PIPES, 100 mM KCl, pH 7.0, T = 25 ºC.

(Fig. 4). As anticipated, Zn(II) can displace from the new probes all the metal ions tested except for Ni(II) and Cu(II), in agreement with the selectivity shown by QZ2, confirming that modification of the quinoline ring does not alter metal-binding selectivity.

Zn(II) Detection in Live Cells. The ability of QZ2E to detect Zn(II) in live cells was investigated using pyrithione as an ionophore to load the metal ion into cells. HeLa cells were incubated with 5 μM QZ2E for 18 h (Fig. 5); 4.5 μM Hoechst 33258 was added 30 min prior to imaging to stain the cell nuclei (Fig. 5b). Very little background fluorescence was observed (Fig. 5c) in the absence of Zn(II), but upon addition of a physiologically relevant concentration of 100 μM Zn:pyrithione (1:1), an immediate increase in fluorescence occurred that maximized within 5 min (Fig. 5d). To ensure that Zn(II) binding of QZ2E induced this fluorescence response, EDTA-$(Et)_4$, a cell-permeable variant of EDTA, was incubated with the cells. For EDTA-$(Et)_4$-induced Zn(II) chelation, and therefore reduction in fluorescence signal to occur, the ester moieties of the chelator must be hydrolyzed intracellularly. Addition of 150 μM EDTA-$(Et)_4$ did not cause an immediate reduction of fluorescence, but after an ~ 5 min incubation period the fluorescence in the green channel was reduced nearly to background levels (Fig. 5e). This

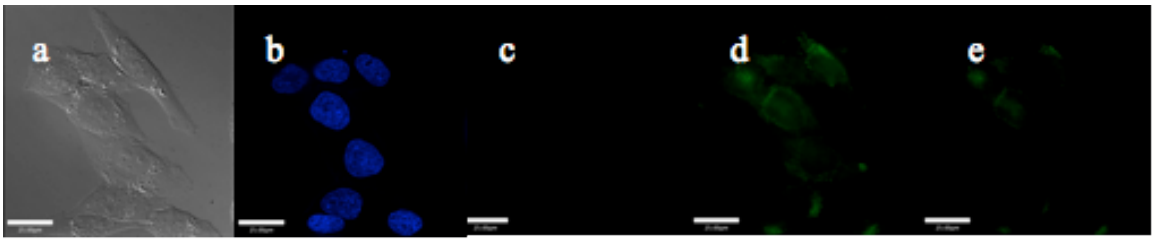

Figure 5. HeLa cells co-incubated with 5 μM QZ2E, and 4.5 μM Hoechst 33258 for 18 h. a) DIC image, b) emission from the blue channel (nuclear stain), c) emission from the green channel (Zn(II) probe), d) emission from the green channel after addition of 100 μM Zn:pyrithione (1:1), and e) emission from the green channel after addition of 150 μM EDTA-$(Et)_4$. Scale bars 25 μm.

result demonstrates that the observed fluorescence is Zn(II)-dependent. A longer incubation period of EDTA-$(Et)_4$ would presumably lead to complete hydrolysis of the chelator and therefore complete reduction of the fluorescence signal in the green channel; however, both the chelator and the ethanol by-product of hydrolysis are toxic to cells, and longer EDTA-$(Et)_4$ incubation periods resulted in cell death.

Cell-Trappability of QZ2E. To demonstrate trappability of the probe, HeLa cells were incubated with 5 μM QZ2E for ~ 18 h to ensure sufficient time for hydrolysis of the ester moieties to produce the cell-impermeable acids (Fig. 6). Addition of 4.5 μM Hoechst 33258 30 min prior to imaging was used to stain the cell nuclei (Fig. 6b). Addition of 100 μM Zn(II):pyrithione (1:1) resulted in a change in fluo-

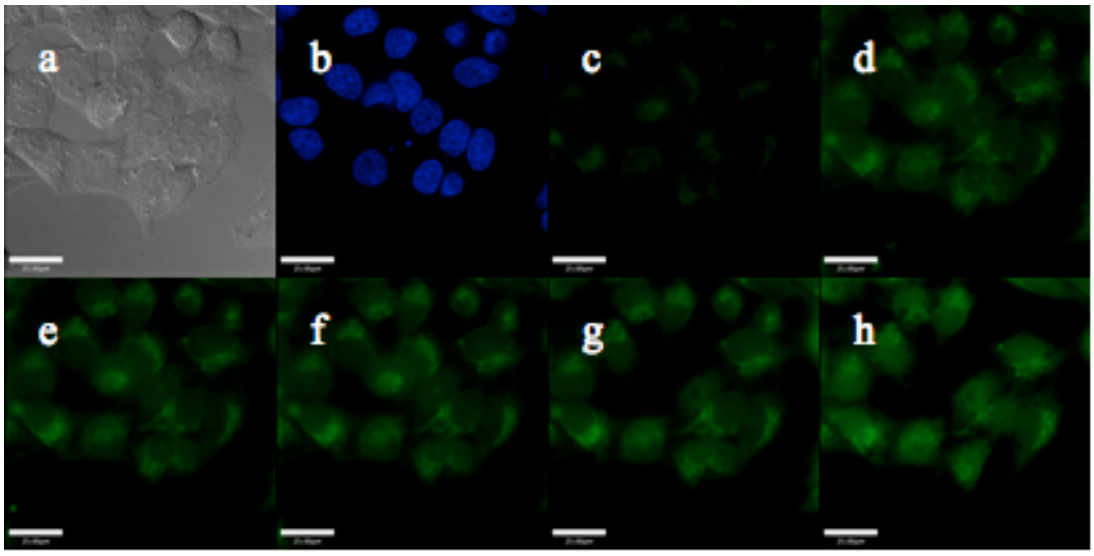

Figure 6. Cell imaging experiments demonstrating retention of QZ2E in HeLa cells co-incubated with 5 μM QZ2E, and 4.5 μM Hoechst 33258 for 18 h. a) DIC image, b) emission from the blue channel (nuclear stain), c) emission from the green channel (Zn(II) probe), d emission from the green channel after addition of 100 μM Zn:pyrithione (1:1) at 5 min, e) 15 min, f) 25 min, g) 35 min, and h) 45 min. Scale bars 25 μm.

rescence from background levels (Fig 6c) to bright green (Fig. 6d) within 5 min. During this time and throughout the experiment, cells were maintained in a microscope incubator at 37 ºC under 5% CO_2 to preserve cell viability. Over the course of 45 min, the cells were periodically washed to mimic conditions of media perfusion. The serum-free DMEM bath was carefully removed by pipette while the plate remained on the microscope and then fresh serum-free DMEM was added. The serum-free DMEM was removed and replaced three times to ensure good washing of the cells, and then removed permanently and replaced with 2 mL of fresh serum-free DMEM. Imaging every 10 minutes over the course of the experiment (Fig. 6e – h) revealed that, under these conditions, Q2E is retained in HeLa cells.

As a further demonstration of cell-trappability, HeLa cells were loaded with 5 μM QZ2A for ~ 18 h with 4.5 μM Hoechst 33258 applied 30 min prior to imaging. Upon washing the cells and imaging, no fluorescent signal was present before or after Zn(II):pyrithione (1;1) addition (Fig. S4). This result is consistent with the hypothesis that the negative charges of the deprotonated carboxylates would prevent QZ2A from entering cells.

QZ2E Localization in HeLa Cells. Like many other fluorescein-based probes, QZ2E shows localization patterns in live cells.[27,47] Punctate staining was observed with clustering in the region surrounding the nuclei, suggesting that QZ2E subcellularly localizes in HeLa cells. To test this hypothesis and determine the organelle of localization, HeLa cells were first coincubated with QZ2E (5 μM), Hoechst 33258 (4.5 μM, nuclear stain), and Mitotracker Red (200 nM, mitochondrial stain), because a probe with a similar structure, Cu_2(FL2E), localizes to mitochondria in SK-N-SH cells.[47] Zn(II):pyrithione (100 μM, 1:1) was added because the green fluorescence could not be visualized adequately without inducing fluorescence enhancement. The results are illustrated in Figs. 7a – e. QZ2E does not enter the nucleus (Fig. 7b, c), as expected, because the negatively charged acids produced upon esterase cleavage of the esters should block passage across the nuclear membrane. An overlay of the green probe fluorescence (Fig. 7c) and the red mitochondrial stain fluorescence (Fig. 7d) indicates very little overlap (Fig. 7e). Most of the red fluorescence persists in the overlay except for a small region of yellow immediately

surrounding the nucleus. These data are inconsistent with QZ2E localization to mitochondria.

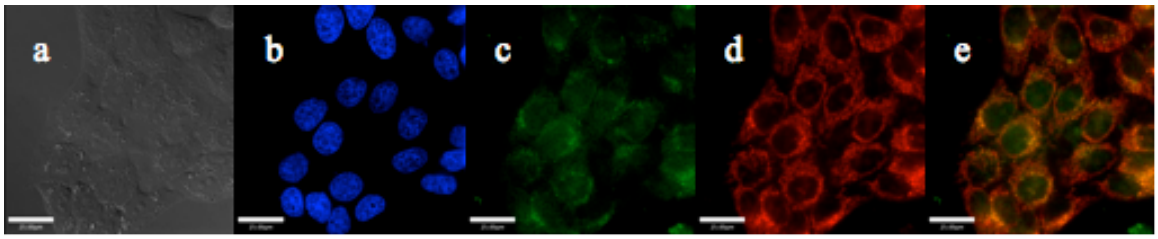

Figure 7. HeLa cells co-incubated with 5 μM QZ2E, 4.5 μM Hoechst 33258, and 200 nM Mitotracker red for 18 h. a) DIC image, b) emission from the blue channel (nuclear stain), c) emission from the green channel (Zn(II) probe) after addition of 100 μM Zn:pyrithione (1:1), d) emission from the red channel (mitochondrial stain), e) overlay of the green and red channels. Scale bars 25 μm.

The Golgi apparatus is another subcellular compartment to which fluorescein-based probes can localize,[27] and is located in close proximity to the nucleus. Therefore, the localization experiments were repeated by incubating HeLa cells with QZ2E (5 μM), Hoechst 33258 (4.5 μM, nuclear stain), and BODIPY TR Ceramide (100 nM, Golgi apparatus stain), and then inducing adequate green fluorescence for visualization with Zn(II):pyrithione (100 μM, 1:1, Fig. 8a – e). In contrast to the results of the mitochondrial staining experiment, an overlay of the green probe fluorescence (Fig. 8c) and the red Golgi stain fluorescence (Fig. 8d) revealed excellent colocalization (Fig. 8e). Essentially all of the red fluorescence observed in Fig, 8d appeared yellow when overlayed with the green QZ2E fluorescence, indicating that QZ2E localizes subcellularly to the Golgi apparatus in HeLa cells. The small overlap of green and red fluorescence observed in Fig. 7e is probably due to mitochondrial and Golgi overlap along the z-axis of the cell and not true localization of QZ2E to mitochondria.

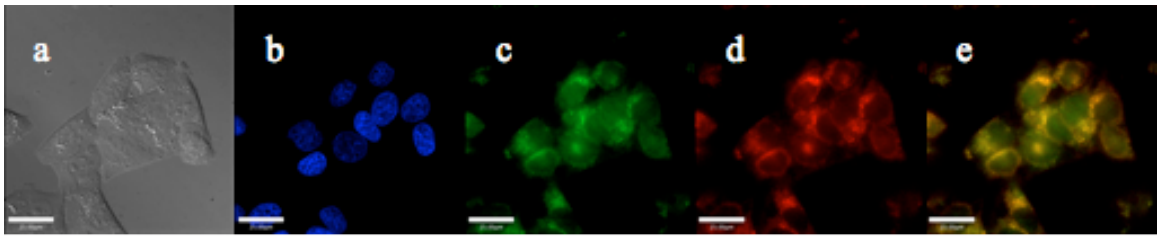

Figure 8. HeLa cells co-incubated with 5 μM QZ2E, 4.5 μM Hoechst 33258, and 100 nM BODIPY TR Ceramide for 18 h. a) DIC image, b) emission from the blue channel (nuclear stain), c) emission from the green channel (Zn(II) probe) after addition of 100 μM Zn:pyrithione (1:1), d) emission from the red channel (Golgi aparatus stain), e) overlay of the green and red channels. Scale bars 25 μm.

Cytotoxicity of QZ2E. Over the course of the cell imaging experiments, there was no visual cell death caused by QZ2E at the concentration used (5 μM); however, the experiments were performed at low probe concentration. To investigate the potential cytotoxic effects of QZ2E at higher concentrations, which may be needed for certain biological applications such as in tissue slices,[47] 3-(4,5-dimethylthiazol-2-yl)-2,5-diphenyltetrazolium bromide (MTT) assays[49] were performed over a 24 hour period. The results indicate that QZ2E is minimally cytotoxic to HeLa cells at concentrations under 25 μM, with ~ 85% cell survival over 24 h for 1 μM probe loading, and ~ 70% cell survival over 24 h for 10 μM QZ2E. At higher concentrations, the probe becomes more toxic. For example, at 25 μM QZ2E the cell survival over 24 h drops to ~ 50%. The cytotoxicity assays are limited by the insolubility of QZ2E in DMSO. Incubation of HeLa cells with 50 μM QZ2E requires a 5% loading of DMSO, which is itself toxic, and therefore cell survival at this concentration over 24 h was only ~ 30%. A control incubation with 5% DMSO and no QZ2E showed similar results (~ 20% cell survival over 24 h), confirming that the addition of DMSO associated with QZ2E application is a limiting factor in QZ2E cytotoxicity.

Summary

The synthesis and spectroscopic characterization of the cell-trappable, fluorescein-based Zn(II) probe QZ2E and its cell-impermeable couterpart, QZ2A, are described. Modifications of the quinoline ring of QZ2E and QZ2A do not drastically alter the Zn(II) binding capacities of the probes when compared to the first generation probe, QZ2 (K_{d1} (QZ2) = 41 ± 3 μM, K_{d1} (QZ2E) = 3.5 ± 0.6 mM, K_{d2} (QZ2E) = 150 ± 100 μM, K_{d1} (QZ2A) = 220 ± 30 μM, K_{d2} (QZ2A) = 160 ± 80 μM, K_{d3} (QZ2A) = 9 ± 6 μM), nor are their emissive properties altered before and after $ZnCl_2$ addition to buffered solutions (ϕ (QZ2) = 0.5%, ϕ (QZ2 + Zn(II)) = 70%; ϕ (QZ2E) = 0.4 ± 0.1%, ϕ (QZ2E + Zn(II)) = 73 ± 3%; ϕ (QZ2A) = 1.2 ± 0.1%, ϕ (QZ2A + Zn(II)) = 51 ± 1%). QZ2E has a slightly reduced dynamic range with respect to QZ2, ~ 120-fold enhancement versus ~ 150-fold enhancement, respectively, but maintains selectivity for Zn(II) over other biologically relevant cations, toxic heavy metals, and most first-row transition metal

ions. The dynamic range of QZ2A is more significantly reduced, to ~ 30-fold enhancement, but this value is more than adequate for in vivo visualization. QZ2E is a competent Zn(II) sensor in live HeLa cells and is retained intracellularly despite numerous washings. Unlike QZ2, QZ2E localizes to the Golgi apparatus in HeLa cells, a difference that may reflect its greater negative charge following intracellular hydrolysis of its ester moieties to become QZ2A.

Acknowledgement. This work was supported by grant CHE-0907905 to SJL from the National Science Foundation (NSF). Spectroscopic instrumentation at the MIT Department of Chemistry Instrument Facility is maintained with funding from NSF grants DBI-9729592 and CHE-9808061. We thank Drs. Elisa Tomat and Daniela Bucella for insightful discussions.

Supporting Information Available: Absorbance spectra for Zn(II) binding of QZ2E and QZ2A; fits with residuals of normalized fluorescence response of QZ2E in the presence of excess Zn(II) fit to eqs 1 and 6; fits with residuals of normalized fluorescence response of QZ2A in the presence of excess Zn(II) fit to eqs 1and 7; QZ2A detection of Zn(II):pyrithione (1:1) in HeLa cells; Full list of authors for Ref. 16. This material is available free of charge via the Internet at http://pubs.acs.org.

TOC Graphic: The trappable Zn(II) fluorescent probe, QZ2E, enters cells where it is hydrolyzed by esterases to form cell-impermeable QZ2A. Following exposure of QZ2A to Zn(II), there is an approximately 30-fold fluorescence enhancement.

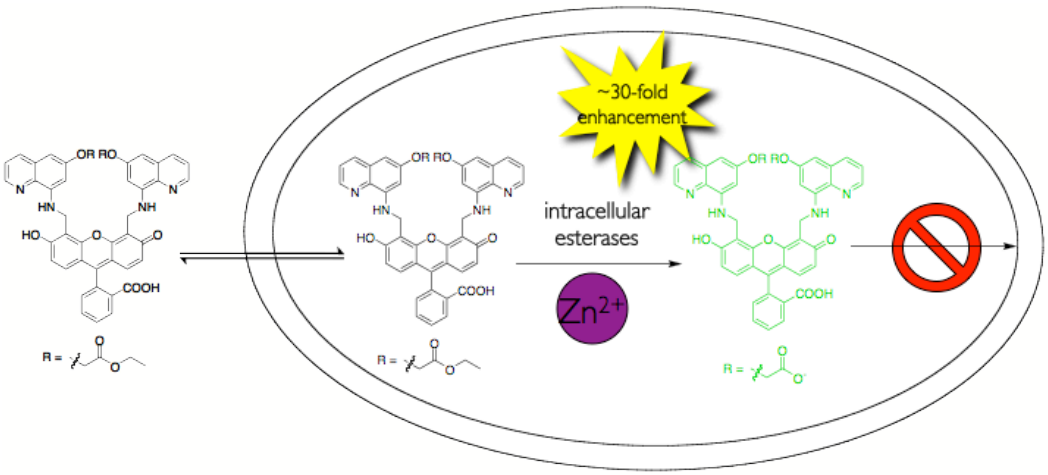
~30-fold
enhancement
intracellular
esterases
Zn2+

References

1. Vallee, B. L.; Falchuk, K. H. *Physiol. Rev.* **1993,** *73*, 79-118.
2. Frederickson, C. J.; Koh, J. Y.; Bush, A. I. *Nature Rev. Neurosci.* **2005,** *6*, 449-462.
3. Maske, H. *Klin. Wochenschr.* **1955,** *33*, 1058.
4. Jo, S. M.; Won, M. H.; Cole, T. B.; Jensen, M. S.; Palmiter, R. D.; Danscher, G. *Brain Res.* **2000,** *865*, 227-236.
5. Costello, L. C.; Franklin, R. B.; Feng, P. *Mitochondrion* **2005,** *5*, 143-53.
6. Mawson, C. A.; Fischer, M. I. *Can. J. Med. Sci.* **1952,** *30*, 336-9.
7. McIsaac, R. J. *Endocrinology* **1955,** *57*, 571-579.
8. Colvin, R. A.; Fontaine, C. P.; Laskowski, G.; Thomas, D. *Eur. J. Pharmacol.* **2003,** *479*, 171-185.
9. Palmiter, R. D.; Cole, T. B.; Quaife, C. J.; Findley, S. D. *Proc. Natl. Acad. Sci. U. S. A.* **1996,** *93*, 14934-14939.
10. Jacob, C.; Maret, W.; Vallee, B. L. *Proc. Natl. Acad. Sci. U. S. A.* **1998,** *95*, 3489-3494.
11. Vallee, B. L. *Neurochem. Int.* **1995,** *27*, 23-33.
12. Galasso, S. L.; Dyck, R. H. *Mol. Med.* **2007,** *13*, 380-387.
13. Bush, A. I.; Pettingell, W. H.; Multhaup, G.; Paradis, M. D.; Vonsattel, J. P.; Gusella, J. F.; Beyreuther, K.; Masters, C. L.; Tanzi, R. E. *Science* **1994,** *265*, 1464-1467.
14. Bush, A. I.; Pettingell, W. H.; Paradis, M. D.; Tanzi, R. E. *J. Biol. Chem.* **1994,** *269*, 12152-12158.
15. Costello, L. C.; Liu, Y. Y.; Zou, J.; Franklin, R. B. *J. Biol. Chem.* **1999,** *274*, 17499-17504.
16. Henshall, S. M.; Afar, D. E. H.; Rasiah, K. K.; Horvath, L. G.; Gish, K.; Caras, I.; Ramakrishnan, V.; Wong, M.; Jeffry, U.; Kench, J. G.; et al. *Oncogene* **2003,** *22*, 6005-6012.
17. Carol, P.; Sreejith, S.; Ajayaghosh, A. *Chem. Asian J.* **2007,** *2*, 338-348.
18. Domaille, D. W.; Que, E. L.; Chang, C. J. *Nat. Chem. Biol.* **2008,** *4*, 168-175.
19. Nolan, E. M.; Lippard, S. J. *Acc. Chem. Res.* **2009,** *42*, 193-203.
20. Que, E. L.; Domaille, D. W.; Chang, C. J. *Chem. Rev.* **2008,** *108*, 1517-1549.
21. Tomat, E.; Lippard, S. J. *Curr. Opin. Chem. Biol.* **2010,** *14*, 225-230.
22. Burdette, S.; Walkup, G.; Spingler, B.; Tsien, R.; Lippard, S. *J. Am. Chem. Soc.* **2001,** *123*, 7831-7841.
23. Chang, C. J.; Nolan, E. M.; Jaworski, J.; Burdette, S. C.; Sheng, M.; Lippard, S. J. *Chem. Biol.* **2004,** *11*, 203-210.
24. Goldsmith, C. R.; Lippard, S. J. *Inorg. Chem.* **2006,** *45*, 6474-6478.
25. Nolan, E. M.; Jaworski, J.; Okamoto, K.-I.; Hayashi, Y.; Sheng, M.; Lippard, S. J. *J. Am. Chem. Soc.* **2005,** *127*, 16812-16823.
26. Nolan, E. M.; Lippard, S. J. *Inorg. Chem.* **2004,** *43*, 8310-8317.
27. Nolan, E. M.; Ryu, J. W.; Jaworski, J.; Feazell, R. P.; Sheng, M.; Lippard, S. J. *J. Am. Chem. Soc.* **2006,** *128*, 15517-15528.
28. Tomat, E.; Nolan, E. M.; Jaworski, J.; Lippard, S. J. *J. Am. Chem. Soc.* **2008,** *130*, 15776-15777.
29. Wong, B. A.; Friedle, S.; Lippard, S. J. *Inorg. Chem.* **2009,** *48*, 7009-7011.
30. Woodroofe, C. C.; Masalha, R.; Barnes, K. R.; Frederickson, C. J.; Lippard, S. J. *Chem. Biol.* **2004,** *11*, 1659-1666.
31. Woodroofe, C. C.; Won, A. C.; Lippard, S. J. *Inorg. Chem.* **2005,** *44*, 3112-3120.
32. Brannon, J. H.; Magde, D. *J. Phys. Chem.* **1978,** *82*, 705-709.
33. Leonhardt, H.; Gordon, L.; Livingston, R. *J. Phys. Chem.* **1971,** *75*, 245-249.
34. Sun, W.-C.; Gee, K. R.; Klaubert, D. H.; Haugland, R. P. *J. Org. Chem.* **1997,** *62*, 6469-6475.
35. Burdette, S. C.; Frederickson, C. J.; Bu, W.; Lippard, S. J. *J. Am. Chem. Soc.* **2003,** *125*, 1778-1787.

36. Chang, C. J.; Nolan, E. M.; Jaworski, J.; Okamoto, K.-I.; Hayashi, Y.; Sheng, M.; Lippard, S. J. *Inorg. Chem.* **2004,** *43*, 6774-6779.
37. Nolan, E. M.; Burdette, S. C.; Harvey, J. H.; Hilderbrand, S. A.; Lippard, S. J. *Inorg. Chem.* **2004,** *43*, 2624-2635.
38. Nolan, E. M.; Jaworski, J.; Racine, M. E.; Sheng, M.; Lippard, S. J. *Inorg. Chem.* **2006,** *45*, 9748-9757.
39. Wong, B. A.; Friedle, S.; Lippard, S. J. *J. Am. Chem. Soc.* **2009,** *131*, 7142-7152.
40. Lim, M. H.; Wong, B. A.; Pitcock, W. H., Jr.; Mokshagundam, D.; Baik, M.-H.; Lippard, S. J. *J. Am. Chem. Soc.* **2006,** *128*, 14364-14373.
41. Lim, M. H.; Xu, D.; Lippard, S. J. *Nat. Chem. Biol.* **2006,** *2*, 375-380.
42. Csuk, R.; Barthel, A.; Brezesinski, T.; Raschke, C. *Eur. J. Med. Chem.* **2004,** *39*, 975-988.
43. Assaf, S. Y.; Chung, S.-H. *Nature* **1984,** *308*, 734-736.
44. Howell, G. A.; Welch, M. G.; Frederickson, C. J. *Nature* **1984,** *308*, 736-738.
45. Chimienti, F.; Favier, A.; Seve, M. *Biometals* **2005,** *18*, 313-317.
46. McQuade, L. E.; Lippard, S. J. *Inorg. Chem.* **2010**, on ASAP, DOI: 10.1021/ic100802q
47. McQuade, L. E.; Ma, J.; Lowe, G.; Ghatpande, A.; Gelperin, A.; Lippard, S. J. *Proc. Natl. Acad. Sci. U. S. A.* **2010,** *107*, 8525-8530.
48. Paoletti, P.; Ascher, P.; Neyton, J. *J. Neurosci.* **1997,** *17*, 5711-5725.
49. Mosmann, T. *J. Immunol. Methods* **1983,** *65*, 55-63.